Applied Surface Science 258 (2012) 7651–7657

Contents lists available at SciVerse ScienceDirect

Applied Surface Science

journal homepage: www.elsevier.com/locate/apsusc

Retardation of surface corrosion of biodegradable magnesium-based materials by aluminum ion implantation

Guosong Wu[a], Ruizhen Xu[a], Kai Feng[a], Shuilin Wu[a], Zhengwei Wu[a], Guangyong Sun[b], Gang Zheng[b], Guangyao Li[b], Paul K. Chu[a,*]

[a] Department of Physics and Materials Science, City University of Hong Kong, Tat Chee Avenue, Kowloon, Hong Kong, China
[b] State Key Laboratory of Advanced Design and Manufacturing for Vehicle Body, Hunan University, Changsha 410082, PR China

ARTICLE INFO

Article history:
Received 2 February 2012
Received in revised form 24 March 2012
Accepted 17 April 2012
Available online 24 April 2012

Keywords:
Magnesium alloys
Biomaterials
Ion implantation
Corrosion
Surface

ABSTRACT

Aluminum ion implantation is employed to modify pure Mg as well as AZ31 and AZ91 magnesium alloys and their surface degradation behavior in simulated body fluids is studied. Polarization tests performed in conjunction with scanning electron microscopy (SEM) reveal that the surface corrosion resistance after Al ion implantation is improved appreciably. This enhancement can be attributed to the formation of a gradient surface structure with a gradual transition from an Al-rich oxide layer to Al-rich metal layer. Compared to the high Al-content magnesium alloy (AZ91), a larger reduction in the degradation rate is achieved from pure magnesium and AZ31. Our results reveal that the surface corrosion resistance of Mg alloys with no or low Al content can be improved by Al ion implantation.

1. Introduction

There has been increasing interest in Mg-based materials for clinical applications such as orthopedics because of natural degradation in the physiological environment and Young's modulus of about 40 GPa similar to that of human bones [1–5]. Proper degradation *in vivo* can obviate the need for a second surgical process to remove the implant from the patient. With regard to traditional biomedical implants made of Ti-based alloys, Co—Cr alloys, and stainless steels, the interface between the implants and affected tissues in the physiological environment is static due to the strong corrosion resistance. However, for biodegradable Mg-based implants, the situation is different because the interface is dynamic and interactions between the implant surface and human tissues as corrosion occur *in situ* [6,7]. Because tissue healing takes time, it is crucial to control the degradation of Mg implants after introduction into the human body. Recently, it has been found in *in vitro* studies that the degradation rate of magnesium-based alloys is high in the initial stage but diminishes significantly with time due to the formation and attachment of corrosion products on the surface [8]. Hence, it is imperative to retard the surface corrosion, especially in the early stage, in order to foster tissue healing.

Surface treatment techniques such as electrochemical deposition [9,10], electroless plating [11,12], conversion [13,14], anodic oxidation [15–19], physical vapor deposition [20–22], and ion implantation [23–25], have been employed to improve the corrosion resistance in aggressive environments. Coatings play an important role in these techniques, but layer delamination and interface mismatch can cause failures and most coatings are non-biocompatible and non-biodegradable. Compared to coatings, ion implantation can introduce a suitable amount of ions into the near surface of the materials to alter the surface properties and owing to the absence of a coating and abrupt interface, delamination is not a serious issue. Zn as a vital element in the human body has been implanted into pure magnesium, but rapid degradation emerges due to galvanic effects [26,27]. If Cr is introduced individually into pure magnesium, a fast degradation similar to that observed after Zn ion implantation appears because Cr exists in the metallic state in the implanted layer. Although ensuing implantation of oxygen produces a thicker surface oxide layer passivating the part of metallic chromium, the retardation of surface degradation is still not desirable [7]. In comparison, metallic Al has an electro-potential close to that of magnesium in aqueous solutions [28] and may be a good candidate. Liu et al. [29] performed Al ion implantation to modify the surface properties of AZ91 magnesium alloy and achieved better corrosion protection than Ti or Zr ion implantation in simulated body fluids.

It is well known that development of new artificial biomaterials is quite time consuming because of stringent requirements

* Corresponding author.
E-mail addresses: paul.chu@cityu.edu.hk, wgshh@sjtu.org, sogohh@sina.com.cn (P.K. Chu).

0169-4332/$ – see front matter © 2012 Elsevier B.V. All rights reserved.
http://dx.doi.org/10.1016/j.apsusc.2012.04.112

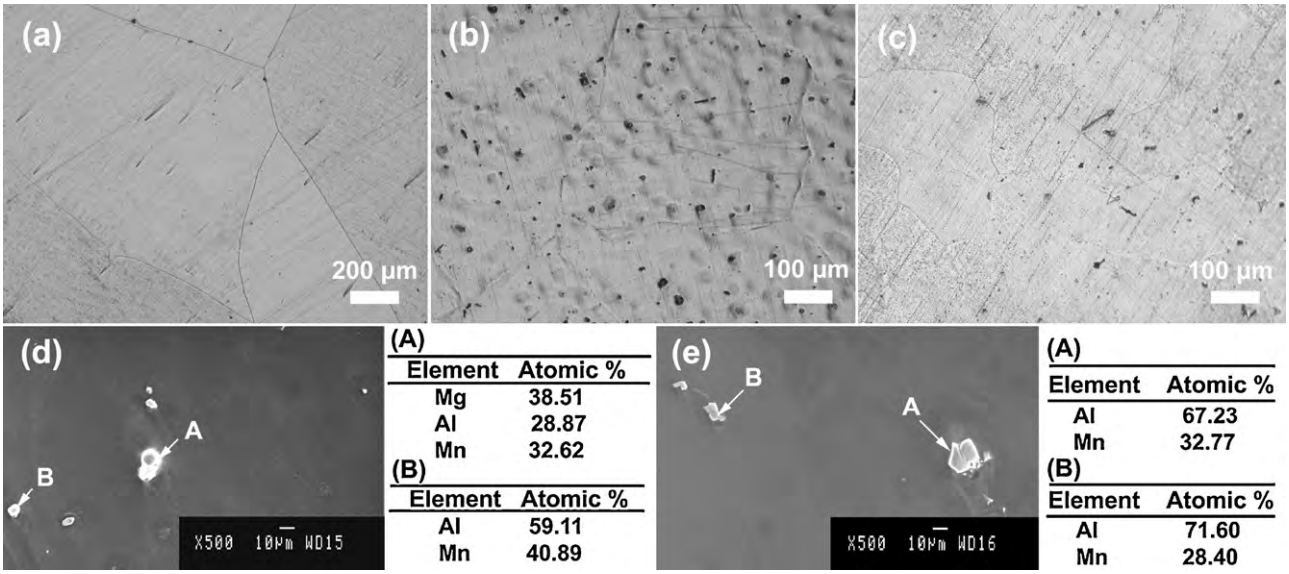

Fig. 1. Optical micrographs of (a) pure magnesium, (b) AZ31 magnesium alloy, and (c) AZ91 magnesium alloy after solution etching. The SEM images and EDS results of the non-matrix phases are shown in (d) AZ31 and (e) AZ91.

imposed by the government, industry, and consumers. Magnesium-based materials are potential useful in bone scaffolds and cardiovascular stents. Different properties such as strength and corrosion resistance are required depending on the location of the biomedical implants in the human body. Therefore, development of biomedical Mg-based alloys is related to the actual requirements. Alloying with Zn and Ca has been proposed in biomedical application [30,31], but excellent corrosion resistance and perfect mechanical properties are still difficult to attain. An alternative method is to select the required alloys from a variety of existing commercial materials such as AZ91, LAE442, and WE43 [32,33] based on less toxicity and better corrosion resistance. In general, addition of Al has been regarded as one of the important alloying methods to improve the corrosion resistance and mechanical properties of magnesium alloys, but an excessively high Al content can indeed be detrimental [34]. If an alloy with no or small aluminum content can meet the requirement for appropriate surface degradation in the initial stage by means of Al ion implantation, the exact Al concentration in the magnesium alloy can then be tailored to yield the optimal mechanical properties. Unfortunately, the effects of Al ion implantation on the surface corrosion resistance of different Mg alloys are still unknown. In this work, we select Mg alloys with different aluminum contents and performed comparative experiments to investigate the surface corrosion resistance after Al ion implantation in simulated physiological conditions.

2. Experimental details

As-cast magnesium (99.95% pure and dimensions of 10 mm × 10 mm × 5 mm), AZ31 (Mg alloy containing 3 wt% Al, 1 wt% Zn, and 0.5 wt% Mn; 10 mm × 10 mm × 5 mm) and AZ91 (Mg alloy containing 9 wt% Al, 1 wt% Zn, and 0.2 wt% Mn; 10 mm × 10 mm × 5 mm) samples were used in this study. After the AZ31 and AZ91 samples were heated at 300 °C and 410 °C, respectively for 24 h, they were quenched in 10 °C pure water to reach a supersaturated state. Their microstructures were determined by optical microscopy (OM) and scanning electron microscopy (SEM). Before microscopic examination, the samples were polished carefully and etched by a solution containing 12 g picric acid, 80 ml acetic acid, 80 ml water, and 350 ml ethanol [35].

Prior to Al ion implantation, the samples were mechanically polished by up to 1 μm diamond paste and ultrasonically washed using pure ethanol. An HEMII-80 ion implanter equipped with an aluminum cathodic arc source manufactured by Plasma Technology Ltd. was used to conduct Al ion implantation. The base pressure in the vacuum chamber was 2×10^{-4} Pa and the implantation time was 1 h. The Al ions were accelerated by a terminal voltage of 35 kV and the nominal ion implantation fluence was 1.6×10^{17} ions cm^{-2}.

Grazing incidence X-ray diffractometry (GIXRD) with an incident beam angle of 1° was used to study the surface crystalline structure of the implanted samples. X-ray photoelectron spectroscopy (XPS) with Al Kα irradiation was used to determine the chemical states and elemental depth profiles after ion implantation. The sputtering rate was estimated to about 13 nm/min as calibrated for SiO_2. The binding energies were referenced to the C 1s line at 285.0 eV.

Simulated body fluids (SBF) [36] were prepared to evaluate the biodegradation behavior. The electrochemical experiment was carried out on a Zahner Zennium electrochemical workstation using the conventional three-electrode technique. The potential was referenced to a saturated calomel electrode (SCE) and the counter electrode was a platinum sheet. The specimens with a surface area of 10 mm × 10 mm were exposed to the SBF and the test was carried out at 1 mV/s scanning rate at 37 °C. The applied potential was scanned from −150 mV to 500 mV *versus* the open circuit potential. After the polarization test, the surface morphology was examined by scanning electron microscopy (SEM).

3. Results

Fig. 1 shows the microstructures of the pure magnesium and magnesium alloy samples. After the solution etching, the grain boundaries are clearly observed *via* optical microscope. It can be further estimated that the grain size of each alloy is about several hundreds micrometers. Even though the solution treatment is applied to every alloy, some non-matrix phases still exist. Energy-dispersive X-ray spectroscopy (EDS) reveals that the black impurities in Fig. 1(b) and (c) are the solid-insoluble Al_xMn_y or $Mg_xAl_yMn_z$ phases. Fig. 2 displays the GIXRD spectra of the unimplanted and implanted samples for $\alpha = 1$, where α is the angle between the surface and incident X-ray. It can be found that the

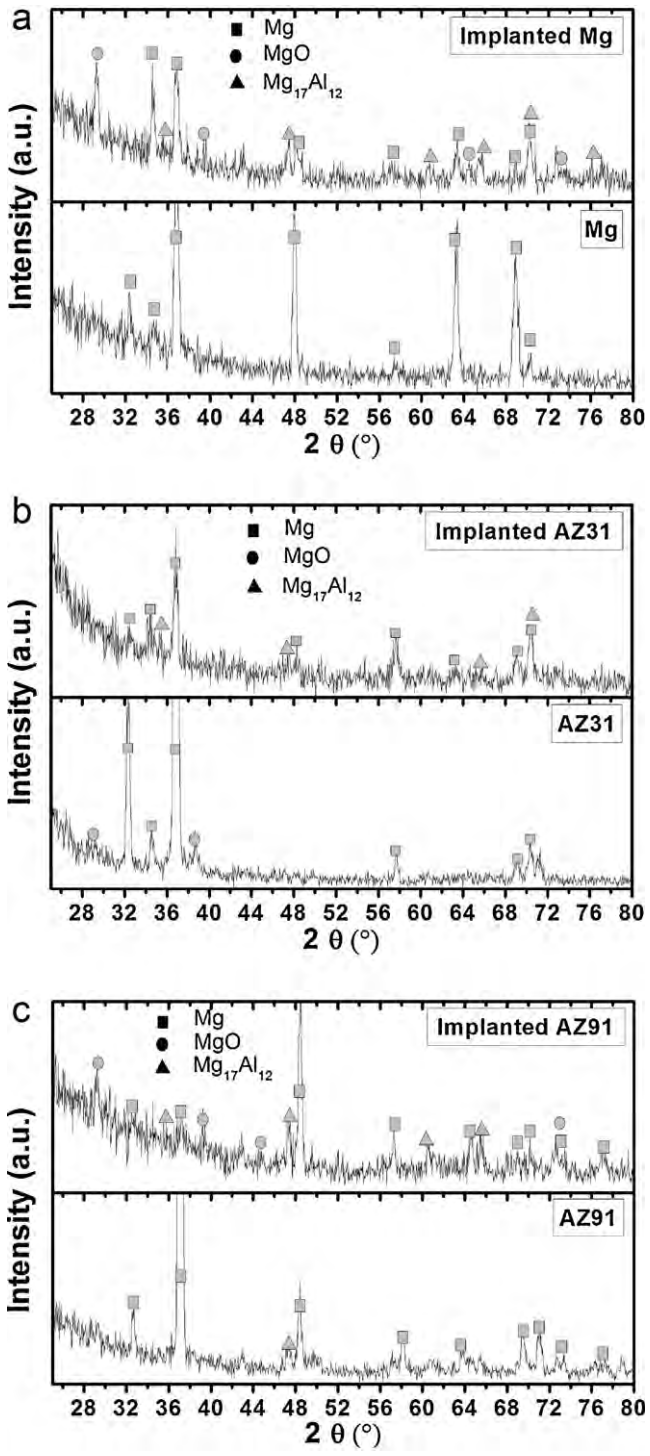

Fig. 2. GIXRD patterns of pure magnesium as well as AZ31 and AZ91 magnesium alloys before and after ion implantation.

$Mg_{17}Al_{12}$ phase is formed in pure Mg as well as AZ31 and AZ91 Mg alloys after Al ion implantation. $Mg(OH)_2$, $MgCO_3$, and MgO are usually formed on the surface of magnesium alloys after exposure to air [37–39], but it is generally difficult to detect them by XRD due to the small amounts. According to the literature [25], one peak of MgO in the XRD pattern has been detected from both un-implanted and Al-implanted magnesium alloys. Here, it is more fortunate in this study that its existence is more accurately inferred by additional peaks in some patterns though the MgO phase does not emerge in all the patterns.

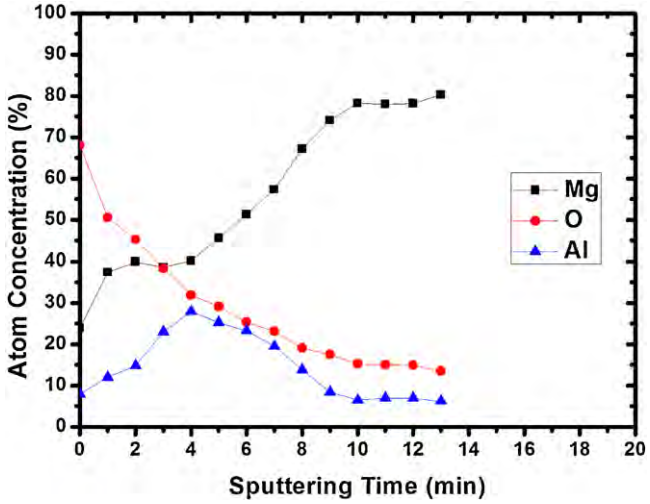

Fig. 3. XPS depth profile of pure magnesium after Al ion implantation.

Fig. 3 depicts the XPS elemental depth profiles of the Al-implanted magnesium disclosing an Al-rich layer near the surface. The maximum Al concentration in the implanted layer is about 28 at% and the O concentration declines gradually with depth. Fig. 4 shows the chemical state changes in the Al-implanted magnesium. The composition of the surface layer is actually quite complex with $Mg(OH)_2$, $MgCO_3$, MgO, and even $MgAl_2O_4$ (Mg 1s: 1304 eV [40]) possibly existing in the implanted layer. It is difficult to ascertain all the compounds by XPS but it is possible to distinguish metallic Mg (or Al) from oxidized Mg (or Al). As shown in the high-resolution XPS spectra, the valence state of Mg gradually changes from the oxidized state to the metallic state with sputtering time and Al also shifts from the oxidized state to metallic state. It can be observed that both Mg and Al are oxidized in the near surface (between sputtering time of 0 min and 1 min) corresponding to a thickness of at least 13 nm. As sputtering proceeds, metallic Al gradually emerges and the depth profiles provide evidence of an Al-rich oxide/Al-rich metal gradient structure. Fig. 5 shows the XPS elemental depth profiles of the Al-implanted AZ31 alloy. The maximum Al concentration in the implanted layer is about 27 at%. Fig. 6 presents the elemental depth profiles acquired from the Al-implanted AZ91 alloy. The maximum Al concentration in the implanted layer is higher than those in pure magnesium and AZ31 possibly due to the high Al concentration in AZ91. For the implanted AZ31 and AZ91, their chemical state changes with depth can be also analyzed using the method described above. It is found that the chemical state changes of Mg and Al with depth exhibit trends similar to those in the implanted pure magnesium.

Fig. 7 displays the polarization curves acquired from pure magnesium, AZ31, and AZ91 in simulated body fluids. As shown in Fig. 7(a), the curve of the Al-implanted magnesium significantly shifts toward a lower current density and nobler potential. In addition, a passive feature occurs in the anodic region of pure magnesium after ion implantation and it can be deduced from the cathodic region that the corrosion current density is reduced from 3.942×10^{-4} to 3.366×10^{-5} A/cm^2. As shown in Fig. 7(b) and (c), the corrosion current density of the Al-implanted AZ31 alloy is similarly reduced from 2.304×10^{-4} to 2.827×10^{-5} A/cm^2 and that of the Al-implanted AZ91 alloy from 1.501×10^{-4} to 5.824×10^{-5} A/cm^2. Hence, a larger reduction in the corrosion current density is observed from pure magnesium and AZ31 compared to AZ91. Moreover, the anodic polarization behavior observed from the samples after ion implantation is significantly different. The Al-implanted Mg sample exhibits a passive-like behavior whereas the un-implanted Mg sample is active in the anodic polarization

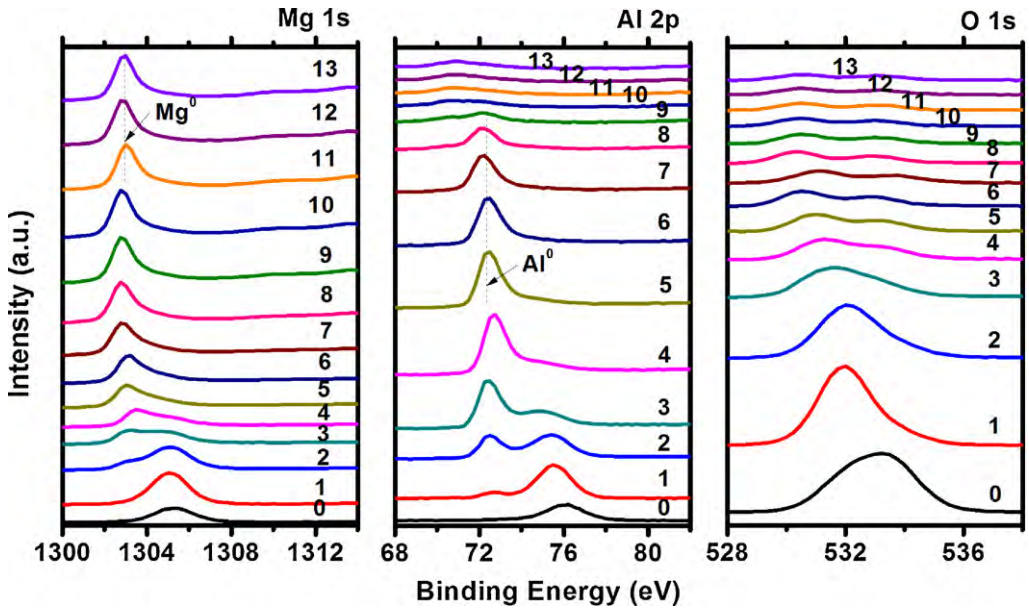

Fig. 4. High resolution XPS spectra of pure magnesium at different sputtering time. The number in the figure denotes the sputtering time.

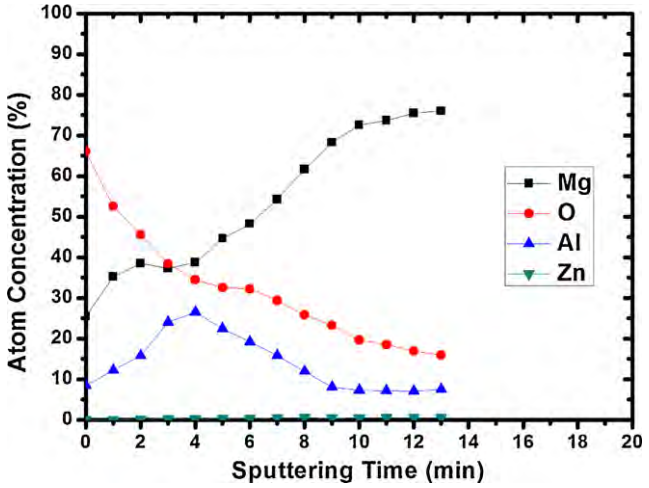

Fig. 5. XPS depth profile of AZ31 magnesium alloy after Al ion implantation.

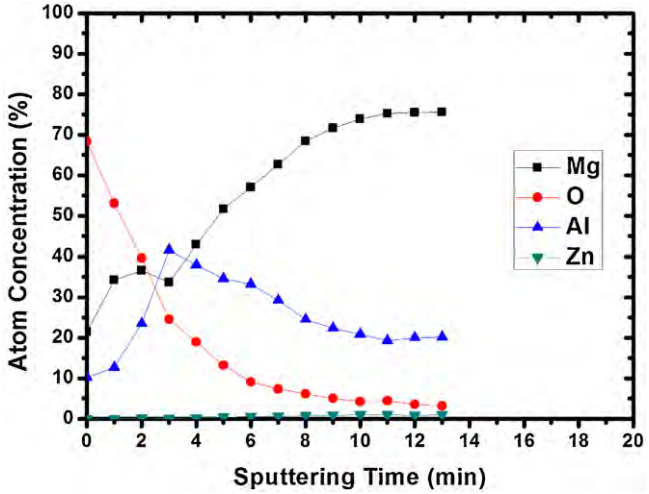

Fig. 6. XPS depth profile of AZ91 magnesium alloy after Al ion implantation.

region. The inverse phenomenon is, however, observed from AZ91. That is, the Al-implanted sample shows an active behavior whereas the un-implanted sample exhibits a passive-like behavior in the anodic polarization region. As for AZ31, the change of the anodic polarization behavior is not as significant as that of pure Mg and AZ91.

Figs. 8–10 depict the SEM micrographs of pure magnesium, AZ31, and AZ91 after the polarization tests, respectively. The surface morphologies of the un-implanted and implanted samples before the polarization test are also shown for comparison. After the polarization tests, web-like cracks can be observed from the surface of the un-implanted sample whereas only pits occur on the Al-implanted samples. Moreover, there are significant differences among the implanted samples after the polarization tests. Compared to the implanted AZ31 and AZ91 alloys, there are more numerous and smaller pits on the surface of the implanted pure magnesium and the results are consistent with the anodic polarization behavior. The presence of chloride ions in SBF will damage the surface oxide film of magnesium to induce random pits. After ion implantation, the stability of the surface oxide film becomes much better. Some weaker micro-regions of the oxide film are preferentially subjected to breaks and develop into pits on the Mg surface at the elevated potential. With regard to AZ31 and AZ91, the surface conditions are more complicated in addition to the existence of second phase revealed to be Al_xMn_y or $Mg_xAl_yMn_z$ in Fig. 1. The difference in the composition between the Al-modified layer and substrate is smaller and then it is possible for the inhomogeneity induced by the second phases to produce weak regions in the corrosion process. After a pit is formed, it will propagate rapidly at the elevated potential during the anodic polarization process.

4. Discussion

According to the polarization tests, both pure magnesium and AZ31 magnesium alloy show larger reduction in the corrosion current density compared to AZ91 after Al ion implantation. The value of pure magnesium (3.366×10^{-5} A/cm^2) and AZ31 magnesium alloy after ion implantation (2.827×10^{-5} A/cm^2) are lower than not only the original value of AZ91 (1.501×10^{-4} A/cm^2) but also AZ91 magnesium alloy after ion implantation (5.824×10^{-5} A/cm^2). Generally, the smaller the corrosion current

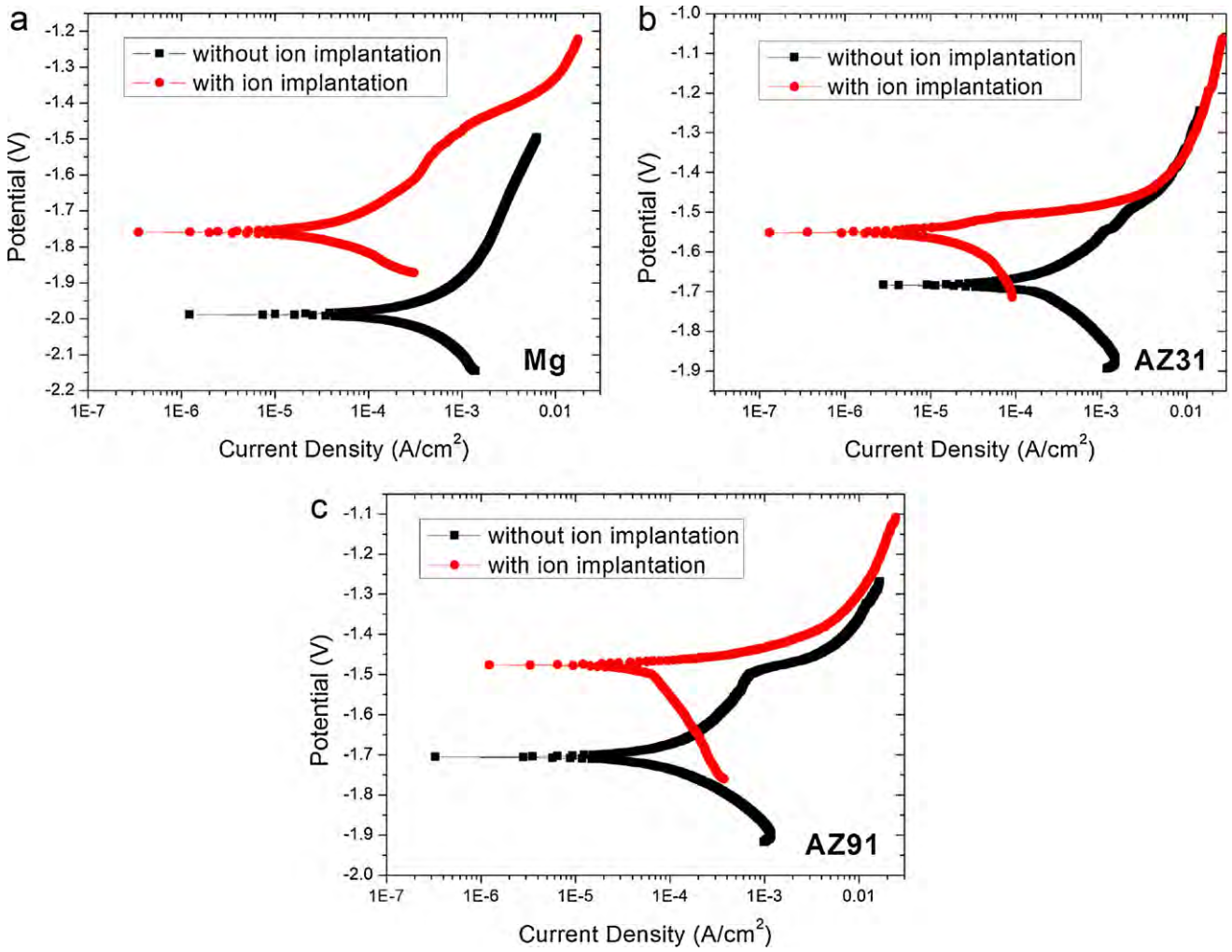

Fig. 7. Polarization curves of (a) pure magnesium, (b) AZ31 magnesium alloy, and (c) AZ91 magnesium alloy in SBF.

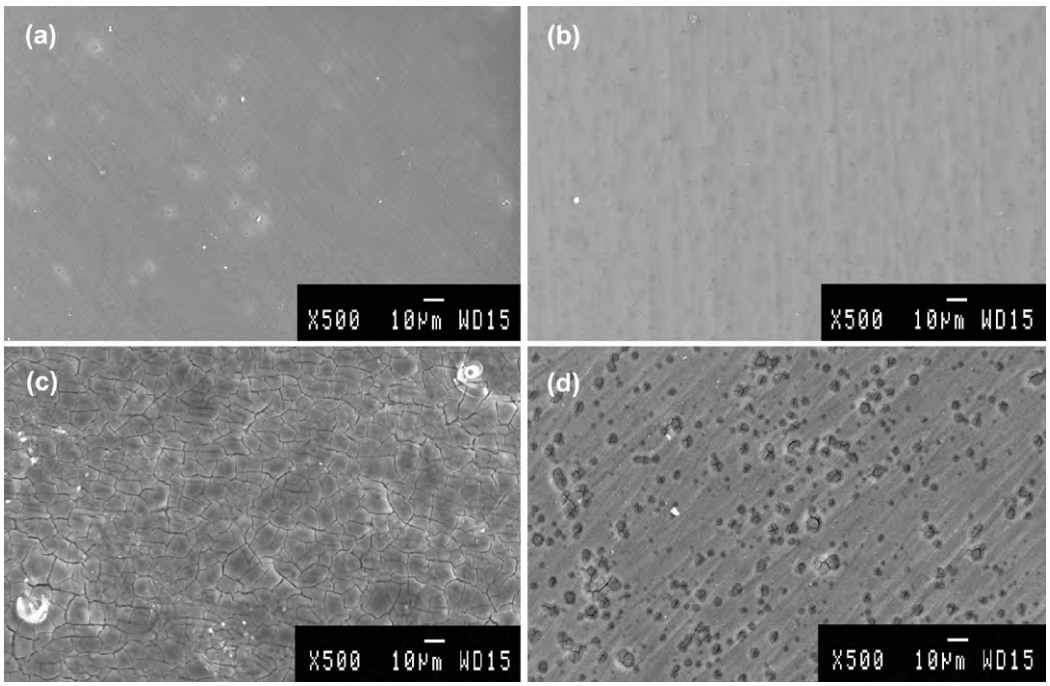

Fig. 8. SEM micrographs of pure magnesium: (a) un-implanted sample before polarization test, (b) implanted sample before polarization test, (c) un-implanted sample after polarization test, and (d) implanted sample after polarization test.

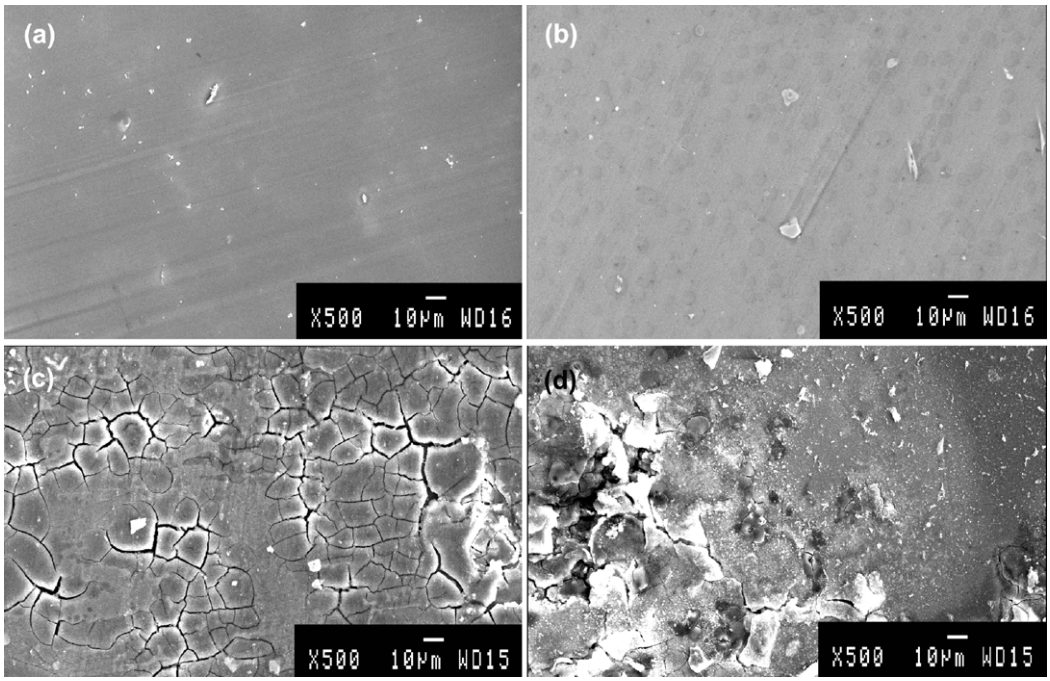

Fig. 9. SEM micrographs of AZ31 magnesium alloy: (a) un-implanted sample before polarization test, (b) implanted sample before polarization test, (c) un-implanted sample after polarization test, and (d) implanted sample after polarization test.

density, the lower is the corrosion resistance. On the surface of the un-implanted sample after corrosion, cracks can be observed. Song et al. [41] proposed that formation of cracks was due to dehydration of the corrosion products when exposed to air. However, after ion implantation, only some pits emerge, implying fewer areas are damaged. The lesser the corrosion products, the lower is the possibility to form cracks. Hence, this is also indirect proof that the corrosion resistance in simulated body fluids is improved after Al ion implantation.

Kirkland et al. [42] discussed the benefits and limitations of current corrosion testing methods including mass loss, hydrogen evolution, polarization, and electrochemical impedance spectroscopy in relation to biodegradable Mg alloys. It was suggested that there was a critical need for investigators to be aware of the salient features of each technique because no single experiment could provide all the information required to understand fully the corrosion behavior of Mg alloys in SBF. Since it typically takes a long time to develop new biomedical materials from scratch, as

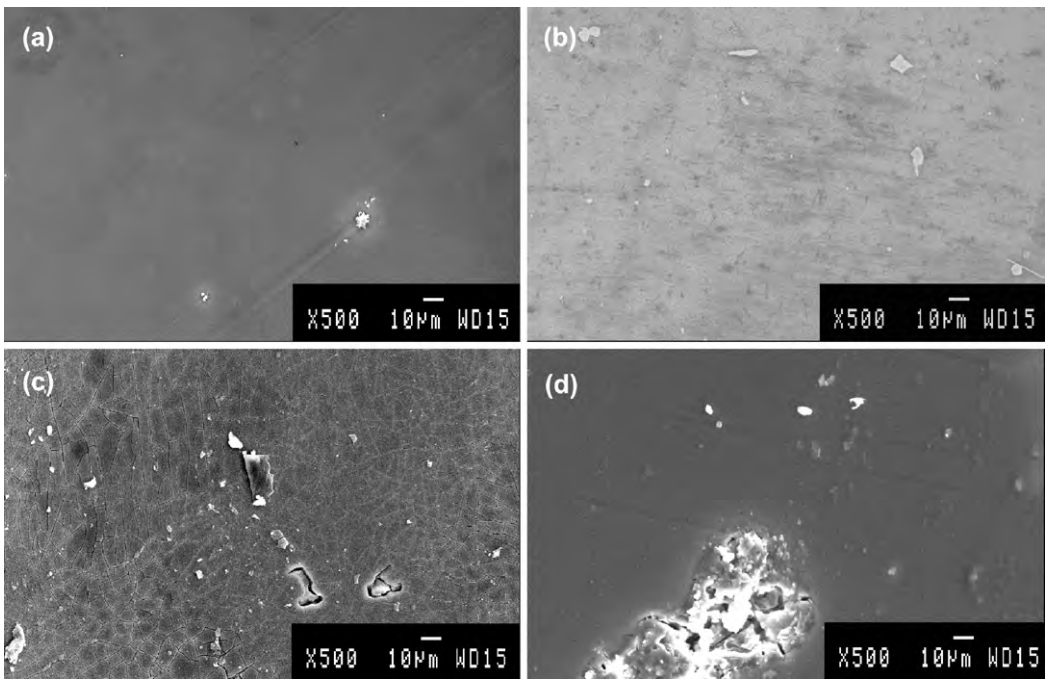

Fig. 10. SEM micrographs of AZ91 magnesium alloy: (a) un-implanted sample before polarization test, (b) implanted sample before polarization test, (c) un-implanted sample after polarization test, and (d) implanted sample after polarization test.

a feasibility study which is the intention of this piece of work, it is more important to find out whether Al ion implantation can indeed enhance the surface corrosion resistance. Only if the surface corrosion resistance is improved when subsequent *in vivo* studies should ensue. Both mass loss and hydrogen evolution experiments are time consuming and strongly affected by anthropic factors. Electrochemical impedance spectroscopy as a real-time monitoring technique is often affected by continuous Mg dissolution at low frequencies and choice of the equivalent circuits. In comparison, polarization is a rapid and convenient method that can be used to not only assess the corrosion resistance but also elucidate the electrochemical corrosion mechanism. After surface modification, the microstructure and composition of the surface layer are very different and in this respect, polarization serves adequately to estimate the surface corrosion resistance qualitatively because it is consistent with immersion tests [43–45]. As discussed earlier, according to the polarization tests and SEM observation, Al ion implantation improves the surface corrosion resistance of pure magnesium and AZ31 to the same extent as AZ91 magnesium alloy, implying that excessive release of Al to the physiological environment can be avoided without compromise of the corrosion resistance if a magnesium alloy with a small bulk concentration of Al is adopted.

Aluminum generally has good corrosion resistance due to the surface passivation layer but the surface film on magnesium is loose offering ineffective protection [20]. It has been observed that a layer of complex oxide film is already formed prior to ion implantation [22,27,37]. During ion implantation, Al ions penetrate the oxide layer and enter the alloy matrix. After ion implantation, a gradient structure consisting of an Al-rich oxide and Al-rich metal is formed near the surface, as evidenced by the previous chemical state analysis. Al exists in the oxidized state in the top layer and gradually transits to the metallic state with depth. The $Mg_{17}Al_{12}$ phase is easily formed in the Al implanted layer according to previous studies [25] and it is also detected by GIXRD in this study. In Mg—Al alloys, the dispersive β-$Mg_{17}Al_{12}$ phase generally acts as a galvanic cathode to accelerate corrosion of the matrix, but if a continuous β-phase network is formed in the matrix, the β-$Mg_{17}Al_{12}$ phase is transformed into a corrosion barrier to hinder corrosion [46]. In other words, $Mg_{17}Al_{12}$ itself can boost the corrosion resistance of magnesium. According to the aforementioned analysis, the top surface layer consists of mainly MgO and Al_2O_3 and the $Mg_{17}Al_{12}$ phase exists in the Al-rich metal layer. The corrosion potential of $Mg_{17}Al_{12}$ is also closer to that of magnesium compared to other metals [46]. Although the modified layer is not very thick, substantial improvement is already noticeable. Therefore, it is a promising surface modification technique for biodegradable magnesium alloys.

5. Conclusion

Al is implanted into pure magnesium as well as AZ31 and AZ91 magnesium alloys to alter the surface corrosion resistance. After Al ion implantation (nominal ion implantation fluence of 1.6×10^{17} ion cm^{-2} at 35 kV terminal voltage), the degradation rates in simulated body fluids are reduced. The formation of a gradient structure in the near surface consisting of an Al-rich oxide layer gradually changing to an Al-rich metal layer is important to the observed improvement in the surface corrosion resistance.

Acknowledgements

This work was financially supported by Hong Kong Research Grants Council (RGC) General Research Funds (GRF) No. CityU 112510 and China Science Funds of State Key Laboratory of Advanced Design and Manufacturing for Vehicle Body No. 31015007. The authors would like to thank Mr. Li Gong (Instrumental Analysis & Research Center, Sun Yat-sen University) for helpful discussion about XPS analysis.

References

[1] E. Zhang, L. Xu, K. Yang, Scripta Materialia 53 (2005) 523.
[2] G. Song, Corrosion Science 49 (2007) 1696.
[3] F. Witte, N. Hort, C. Vogt, S. Cohen, K.U. Kainer, R. Willumeit, F. Feyerabend, Current Opinion on Solid State Material Science 12 (2008) 63.
[4] B. Zberg, P.J. Uggowitzer, J.F. Löffler, Nature Materials 8 (2009) 887.
[5] X. Gu, Y. Zheng, Y. Cheng, S. Zhong, T. Xi, Biomaterials 30 (2009) 484.
[6] G. Wu, K. Feng, A. Shanaghi, Y. Zhao, R. Xu, G. Yuan, P.K. Chu, Surface and Coatings Technology 206 (2012) 3186.
[7] R. Xu, G. Wu, X. Yang, T. Hu, Q. Lu, P.K. Chu, Materials Letters 65 (2011) 2171.
[8] Y. Xin, C. Liu, X. Zhang, G. Tang, X. Tian, P.K. Chu, Journal of Materials Research 22 (2007) 2004.
[9] J. Zhang, C. Yan, F. Wang, Applied Surface Science 255 (2009) 4926.
[10] S. Zhang, F. Cao, L. Chang, J. Zheng, Z. Zhang, J. Zhang, C. Cao, Applied Surface Science 257 (2011) 9213.
[11] C. Gu, J. Lian, G. Li, L. Niu, Z. Jiang, Journal of Alloys and Compounds 391 (2005) 104.
[12] W. Zhang, Z. Jiang, G. Li, Q. Jiang, J. Lian, Applied Surface Science 254 (2008) 4949.
[13] Z. Yong, J. Zhu, C. Qiu, Y. Liu, Applied Surface Science 255 (2008) 1672.
[14] F. Pan, X. Yang, D. Zhang, Applied Surface Science 255 (2009) 8363.
[15] H. Guo, M. An, Applied Surface Science 246 (2005) 229.
[16] C. Wu, Z. Zhang, F. Cao, L. Zhang, J. Zhang, C. Cao, Applied Surface Science 253 (2007) 3893.
[17] J. Liang, L. Hu, J. Hao, Applied Surface Science 253 (2007) 4490.
[18] X. Wang, L. Zhu, W. Li, H. Liu, Y. Li, Applied Surface Science 255 (2009) 5721.
[19] C. Blawert, V. Heitmann, W. Dietzel, H. Nykyforchyn, M. Klapkiv, Surface and Coatings Technology 200 (2005) 68.
[20] G. Wu, X. Zeng, W. Ding, X. Guo, S. Yao, Applied Surface Science 252 (2006) 7422.
[21] G. Wu, X. Zeng, G. Li, S. Yao, X. Wang, Materials Letters 60 (2006) 674.
[22] G. Wu, K. Ding, X. Zeng, X. Wang, S. Yao, Scripta Materialia 61 (2009) 269.
[23] X. Wang, X. Zeng, G. Wu, S. Yao, Applied Surface Science 253 (2006) 2437.
[24] X. Wang, X. Zeng, G. Wu, S. Yao, Y. Lai, Journal of Alloys and Compounds 437 (2007) 87.
[25] M. Lei, P. Li, H. Yang, X. Zhu, Surface and Coatings Technology 201 (2007) 5182.
[26] Y. Wan, G. Xiong, H. Luo, F. He, Y. Huang, Y. Wang, Applied Surface Science 254 (2008) 5514.
[27] G. Wu, L. Gong, K. Feng, S. Wu, Y. Zhao, P.K. Chu, Materials Letters 65 (2011) 661.
[28] J. Zhang, W. Zhang, C. Yan, K. Du, F. Wang, Electrochimica Acta 55 (2009) 560.
[29] C. Liu, Y. Xin, X. Tian, P.K. Chu, Thin Solid Films 516 (2007) 422.
[30] X. Gu, Y. Zheng, S. Zhong, T. Xi, J. Wang, W. Wang, Biomaterials 31 (2010) 1093.
[31] J. Li, Y. Song, S. Zhang, C. Zhao, F. Zhang, X. Zhang, L. Cao, Q. Fan, T. Tang, Biomaterials 31 (2010) 5782.
[32] F. Witte, J. Fischer, J. Nellesen, H. Crostack, Volker Kaese, A. Pischd, F. Beckmann, H. Windhagen, Biomaterials 27 (2006) 1013.
[33] Y. Zhao, G. Wu, H. Pan, W. Yeung, P.K. Chu, Materials Chemistry and Physics 132 (2012) 187.
[34] M.B. Kannan, R.K. Singh Raman, Biomaterials 29 (2008) 2306.
[35] P. Fu, L. Peng, H. Jiang, L. Ma, C. Zhai, Materials Science and Engineering A 496 (2008) 177.
[36] C. Liu, Y. Xin, X. Tian, J. Zhao, P.K. Chu, Journal of Vacuum Science and Technology A 25 (2007) 334.
[37] G. Wu, X. Zeng, G. Yuan, Materials Letters 62 (2008) 4325.
[38] M. Liu, S. Zanna, H. Ardelean, I. Frateur, P. Schmutz, G. Song, A. Atrens, P. Marcus, Corrosion Science 51 (2009) 1115.
[39] M. Santamaria, F.D. Quarto, S. Zanna, P. Marcus, Electrochimica Acta 53 (2007) 1314.
[40] J.F. Moulder, W.F. Stickle, P.E. Sobol, K.D. Bomben, J. Chastain, Handbook of X-ray Photoelectron Spectroscopy, Perkin-Elmer Corporation, Physical Electronics Division, Minnesota, USA, 1992.
[41] Y. Song, D. Shan, R. Chen, F. Zhang, E. Han, Materials Science and Engineering C 29 (2009) 1039.
[42] N.T. Kirkland, N. Birbilis, M.P. Staiger, Acta Biomaterial 8 (2012) 925.
[43] Y. Song, D. Shan, R. Chen, F. Zhang, E. Han, Surface and Coatings Technology 203 (2009) 1107.
[44] W. Dai, G. Wu, A. Wang, Diamond and Related Materials 19 (2010) 1307.
[45] Y. Xin, C. Liu, W. Zhang, J. Jiang, G. Tang, X. Tian, P.K. Chu, Journal of the Electrochemical Society 155 (2008) C178.
[46] G. Song, A. Atrens, Advanced Engineering Materials 5 (2003) 837.